Journal of
Medicinal Chemistry

Article

Structural studies on the inhibitory binding mode of aromatic coumarinic esters to human kallikrein-related peptidase 7

Stefanie Hanke, Catherine Tindall, Jan Pippel, David Ulbricht, Bernard Pirotte, Michele Reboud- Ravaux, John T Heiker, and Norbert Sträter

J. Med. Chem., **Just Accepted Manuscript** • DOI: 10.1021/acs.jmedchem.9b01806 • Publication Date (Web): 06 May 2020

Structural studies on the inhibitory binding mode of aromatic coumarinic esters to human kallikrein-related peptidase 7

Stefanie Hanke[§], Catherine A. Tindall[†], Jan Pippel[§], David Ulbricht[†], Bernard Pirotte[‡], Michèle Reboud-Ravaux[‖], John T. Heiker[†,⊥,ǀ], Norbert Sträter*[,§]

[§] Institute of Bioanalytical Chemistry, Center for Biotechnology and Biomedicine, Leipzig University, Deutscher Platz 5, 04103 Leipzig, Germany

[†] Institute of Biochemistry, Faculty of Life Sciences, Leipzig University, Brüderstrasse 34, 04103 Leipzig, Germany

[‡] Laboratory of Medicinal Chemistry, Center for Interdisciplinary Research on Medicines (CIRM), University Liège, Avenue Hippocrate 15, 4000 Liège, Belgium

[‖] Sorbonne Université, CNRS, INSERM, Institut de Biologie Paris Seine, IBPS, Adaptation biologique et Vieillissement, 7 quai Saint Bernard, 75252 Paris Cedex 05, France

[⊥] IFB Adiposity Diseases, Leipzig University, Liebigstr. 19, 04103 Leipzig, Germany

[ǀ] Helmholtz Institute for Metabolic, Obesity and Vascular Research (HI-MAG) of the Helmholtz Zentrum München at Leipzig University and University Hospital Leipzig, Philipp-Rosenthal-Str. 27, 04103 Leipzig, Germany

Abstract

The serine protease kallikrein-related peptidase 7 (KLK7) is a member of the human tissue kallikreins. Its dysregulation leads to pathophysiological inflammatory processes in the skin. Furthermore, it plays a role in several types of cancer. For the treatment of KLK7-associated diseases, coumarinic esters have been developed as small molecule enzyme inhibitors. To characterize the inhibition mode of these inhibitors, we analyzed structures of the inhibited protease by X-ray crystallography. Electron density shows the inhibitors covalently attached to His57 of the catalytic triad. This confirms the irreversible character of the inhibition process. Upon inhibitor binding His57 undergoes an outward rotation thus the catalytic triad of the protease is disrupted. Besides, the halophenyl moiety of the inhibitor was absent in the final enzyme-inhibitor complex due to hydrolysis of the ester linkage. With these results, we analyze the structural basis of KLK7 inhibition by covalent attachment of aromatic coumarinic esters.

Introduction

Human kallikrein-related peptidase 7 (KLK7), also known as stratum corneum chymotryptic enzyme, is a member of the human tissue kallikreins, a protein family containing 15 chymotrypsin- or trypsin-like serine proteases[1–3]. Tissue kallikreins are expressed in various tissues such as skin, pancreas, breast, and prostate, whereas KLK7 is predominantly expressed in the outer layer of the skin[4–6]. KLK7 regulates desquamation of the skin by degradation of the intercellular adhesion molecules corneodesmosin, desmoglein 1 and desmocollin 1[7–10]. Its dysregulation leads to pathophysiological inflammatory processes in the skin, causing diseases such as psoriasis, chronic dermatitis and Netherton Syndrome[11,12]. However, KLK7 is also associated with tumor progression in melanoma, breast, ovarian, prostate and other cancer types[13]. To date, the distinct role of KLK7 in tumor progression is poorly defined, but it may facilitate tumor cell invasion as described for pancreatic cancer[14]. Aberrant KLK7 expression serves as a therapeutic marker for malignant melanoma[15]. Recently, KLK7 activity has also been linked to adipose tissue inflammation and systemic insulin resistance in obesity[16].

Mature KLK7 consists of a typical serine protease domain with Ser195, His57 and Asp102 as the catalytic triad. These residues form the entrance to the specificity pocket S1, which is the main region of substrate binding and cleavage. The oxyanion hole is formed by the backbone amides of Ser195 and Gly193. KLK7 has an Asn at position 189. Most kallikreins have Asp189 at the bottom of the S1 pocket, but this residue differs also in KLK3 (Ser), KLK9 (Gly) and KLK15 (Glu). The S1 pocket can accommodate medium- to large- amino acid side chains with polar tips, but Arg and Lys are predominantly accommodated. In addition to the main specificity pocket S1, subsites S2- S4 and S1'- S4'contribute to substrate recognition[17].

Its pathophysiological role makes KLK7 an interesting drug target and many efforts have been made to develop KLK7-specific inhibitors for therapeutic uses. Current KLK7 inhibitors can be categorized into physiological and non-physiological inhibitors. Physiological inhibitors such as metal ions or endogenous protein inhibitors are essential to maintain the homeostasis of kallikrein activity. The best-characterized endogenous protein inhibitor of KLK7 is the serpin vaspin (SERPINA12), which belongs to the superfamily of serine protease inhibitors[18,19]. Another well-characterized endogenous inhibitor is LEKTI, a Kazal-type serine protease inhibitor encoded by the SPINK5 gene[6,20].

For pharmaceutical purposes**,** non-physiological inhibitors of kallikreins have been developed as natural peptides and proteins[21], natural heterocyclic compounds, synthetic peptides[22] and non-peptidic compounds[23]. The latter include coumarin-3-carboxylate derivatives, which act as inhibitors for certain kallikreins, α-chymotrypsin, human leukocyte elastase and matriptase[24–27]. Non-peptidic synthetic derivatives are very promising pharmacological tools as they can usually be developed to small molecules (Mw < 800 Da) with high target selectivity, good bioavailability and chemical stability. Information for structure-based inhibitor development is available for unliganded KLK7[28] and also complexes with several competitive inhibitors[29–32].

Coumarin-3-carboxylate derivatives were first developed to inhibit α-chymotrypsin in a suicide manner[24,25]. Recently, Tan *et al.* optimized these compounds for KLK7 inhibition as aromatic coumarinic esters to increase potency and selectivity[26]. Some of these optimized derivatives inhibit KLK7 with apparent IC_{50}

values in the nM range (at an enzyme concentration of 7.6 nM and a reaction time of 15 min), are non-toxic on keratinocytes, and thus are promising drug candidates to treat Netherton syndrome (Figure 1). It has been suggested that these compounds are attacked at the lactone ester bond by the Ser195 nucleophile of KLK7 and an acyl-enzyme intermediate is formed. Expulsion of the aliphatic chlorine results in a quinone methide, which induces alkylation of His57 of the catalytic triad[26]. Thus, these inhibitors act in a suicide manner and inhibit KLK7 irreversibly. Docking studies have been used to characterize the initial non-covalent inhibitor binding mode prior to nucleophilic attack of Ser195 and for the analysis of structure-activity relationships[33,26].

Here, we analyze crystal structures of KLK7 in complex with this class of suicide inhibitors for a better understanding of the inhibitory mechanism of aromatic coumarinic esters and to contribute to further inhibitor development (Figure 1).

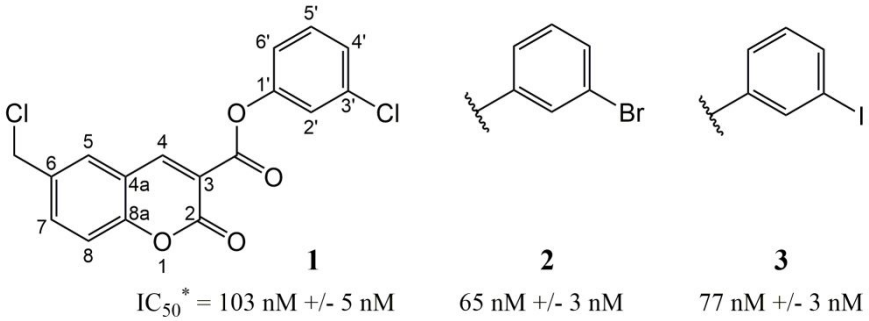

Figure 1. **Aromatic coumarinic esters studied in this work**. The compounds shown here were first reported by Tan *et al.*, 2015[26] and (from left to right) refer to the compounds **11**, **22** and **23** of their study. The apparent IC_{50}* values of the covalent inhibitors were determined at an enzyme concentration of 7.6 nM and a reaction time of 15 min.

Results

Protease stability under inhibition conditions. The inhibitor molecules investigated in this study have a limited solubility in water due to hydrophobicity and thus addition of the solvent DMSO was necessary to incubate KLK7 with higher inhibitor concentrations. We therefore characterized the stability of KLK7 in the presence of DMSO. The thermal melting point (T_m) of KLK7 was determined by differential scanning fluorimetry (DSF) at 0 % – 60 % DMSO (v/v) (Figure 2). A continuous decrease of the T_m was observed

with increasing DMSO concentration and we chose a DMSO concentration of 10 % (v/v) or lower for our experiments. Analysis of the time dependence of KLK7 stability at 10 % DMSO concentration showed no further destabilization of the protease at prolonged incubation times up to 17 h at room temperature (data not shown). Likewise, after preincubation of KLK7 for 30 min at 37 °C the T_m was only slightly reduced from 58.6 °C (no preincubation of the enzyme) to 56.1 °C. These findings demonstrate sufficient stability of the protease under conditions of the compound inhibition experiments.

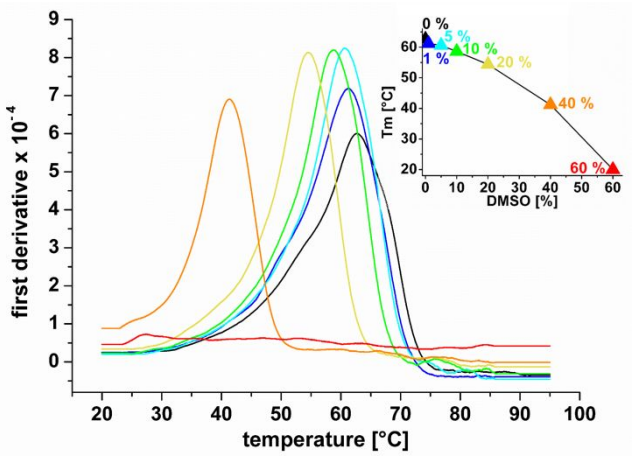

Figure 2. **Thermal stability of KLK7 in the presence of DMSO.** The melting point (T_m) of KLK7 was determined by DSF in a buffer consisting of 50 mM sodium phosphate, pH 7.5, and increasing concentrations of DMSO. The first derivative of the F350/F330 fluorescence ratio was plotted against the temperature. T_m is determined from the maxima of these curves, which are colored according to the different DMSO concentrations as indicated in the insert. The insert shows the decrease of T_m in relation to the DMSO concentration.

Inhibition of KLK7-vaspin complex formation. We next verified the proteolytic inactivity of the KLK7-inhibitor complexes prior to crystallization. Therefore, we analyzed the putative remaining activity with the KLK7 target vaspin. In the absence of inhibitors the covalent KLK7-vaspin complex is readily formed, whereas little or no complex formation is observed for the inhibited protease preparations (Figure 3). This is in agreement with the previously observed covalent inhibition of KLK7 by the coumarinic derivatives[26]. In addition to complex formation with vaspin, active KLK7 also specifically cleaves after Tyr30 within the N-terminus of vaspin (Figure 3). This N-terminal cleavage was also observed for the inhibited KLK7 preparations, most likely due to the long reaction time of 60 min and based on traces of uninhibited KLK7

or residual activity of the inhibited enzyme. The much higher catalytic efficiency of N-terminal processing compared to cleavage of the reactive center loop of vaspin (and complex formation) has been noticed previously[18]. In addition, activity measurements using NFF-3 peptide (see experimental section) showed that the protease activity is reduced from > 400 (pmol/min)/µg protease to values < 0.1 (pmol/min)/µg.

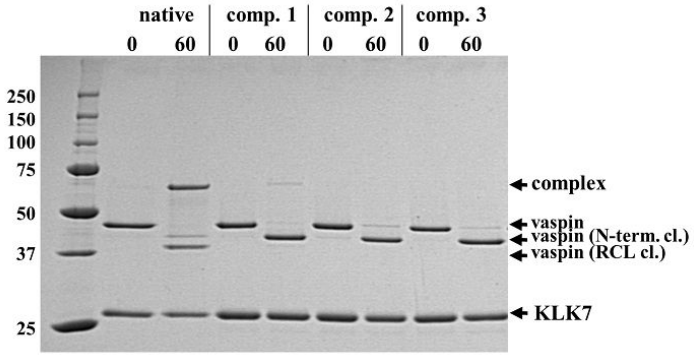

Figure 3. **Inhibition of complex formation of KLK7 with vaspin by compounds 1, 2, and 3.** A Coomassie-stained SDS-PAGE gel was prepared after the incubation of active and inhibited KLK7 with vaspin for 0 and 60 minutes (see experimental section for details). Active KLK7 forms a covalent complex with vaspin (70 kDa). After incubation with compounds **1**, **2** or **3**, only traces of complexes or no complexes at all are detected for inhibited KLK7. comp. = compound, N-term. cl. = N-terminally cleaved.

Crystal structures of KLK7 after incubation with aromatic coumarinic esters. Crystal structures of the three inhibited KLK7 preparations were analyzed between 1.85 Å and 2.02 Å resolution (Table 1). The key structural features of the binding mode of all three compounds are rather similar, therefore we describe the crystal structure with compound **2**, which was analyzed to the highest resolution and is the most potent of the three inhibitors. The crystals of space group $P2_12_12_1$ contain eight molecules in the asymmetric unit, which have similar structures and differ by less than 0.2 Å root mean square deviation (rmsd). For all eight copies, two protease molecules face each other by their active site cleft (Figure S1). We also crystallized unliganded KLK7 and obtained the same crystal form as previously described (pdb id 3BSQ[28]), but could improve the resolution from 2.8 to 2.3 Å (Table 1). Covalent inhibition of KLK7 by compounds **1-3** does

not induce overall structural changes, as inhibited and unliganded KLK7 superimpose with an rmsd of 0.37 Å (Figure S1C).

In the crystal structures, the bound inhibitor moiety is devoid of the halogenated phenyl group present in the starting molecule, whereas a free carboxylate group is located at position 3 of the coumarinic scaffold (Figure 4). This indicates that the corresponding exocyclic ester has been hydrolyzed during the experimental processes. In all cases, the inhibitor is covalently attached to the N_{δ}-atom of His57 and is present in two alternative conformations (A and B) within the active site cleft (Figure 4). The His57-N_{δ}-atom forms a covalent bond with the methylene group in the 6-position of the inhibitor and thus replaces the aliphatic chlorine atom. Conformation A points alongside the specificity pockets S1'- S3'. The 3-carboxylate of conformation A forms a hydrogen bond with the backbone amide of Gly193 occupying the oxyanion hole, known to accommodate the tetrahedral intermediate during the attack of the substrates' scissile peptide bond by Ser195 (Figure 4)[34]. Conformation B points towards the specificity pocket S2, which is formed mainly by the residues Trp215 and His99[17]. The 3-carboxylate of conformation B forms a hydrogen bond with the backbone amide of Gly216 (Figure 4). The two conformations were refined to almost equal occupancies (0.49 for conformation A and 0.51 for conformation B) and both conformations are involved in crystal packing contacts. The inhibitors in conformation B of the crystal packing dimer form a π-stacking interaction (Figure 4D). Both inhibitor conformations do not form any clashes concerning contacts with each other and the models suggest that all four inhibitor orientations conceivable for the packing dimer might be possible. The postulated complex[26] with the dual attachment to the active site through Ser195 and His57 is not observed in the crystal structure. Nevertheless, an initial nucleophilic attack by Ser195 is necessary to demask the reactive alkylating function. A subsequent hydrolysis of the formed ester bond has thus occurred.

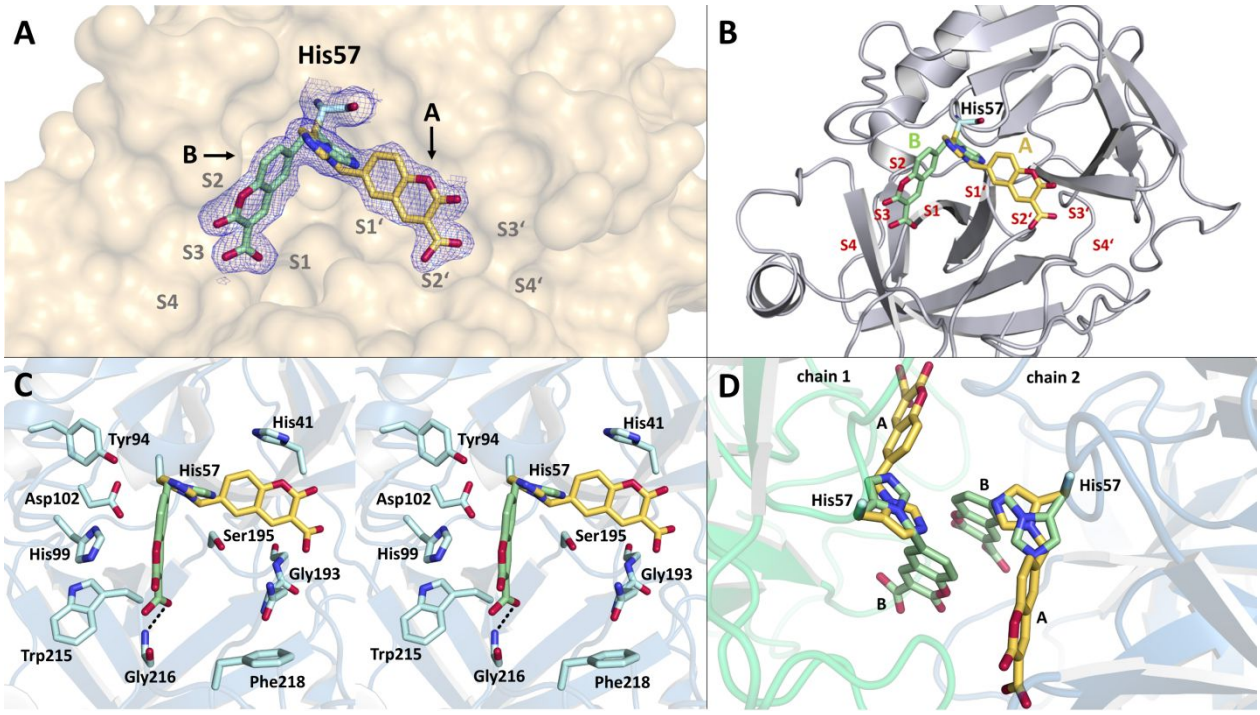

Figure 4. **Crystal structure of KLK7 in complex with compound 2 (PDB code 6SHI).** The specificity pockets of KLK7 are labeled S1-S4 and S1'-S4'. Hydrogen bonds are displayed as black dashed lines. (A) Active site cleft of KLK7 with compound **2** bound to His57. The electron density of the (2Fo-Fc)-type map is shown in blue at a contour level 0.7 σ. The inhibitor is present in two alternative conformations (A in yellow and B in green). (B) Cartoon representation. (C) Stereo figure of the amino acids in the inhibitor environment. A similar figure showing the two inhibitor conformations separately can be found as Figure S2. (D) Inhibitor conformations B form π-stacking interactions between two KLK7 chains.

The crystal structure of unliganded KLK7 in space group H32 was analyzed to a resolution of 2.2 Å (Table 1). A comparison of the inhibited and unliganded KLK7 structures shows two major differences. Compared to the catalytic triad of unliganded KLK7 the His57 sidechain undergoes an outward rotation around the Cα-Cβ bond, whereby the catalytic triad is disrupted in the inhibited protease (Figure 5A). In addition, His99 adopts a new conformation compared to the unliganded KLK7 structure to avoid closed contacts to the inhibitor in conformation B and to the rotated His57 in conformation A (Figure 5B).

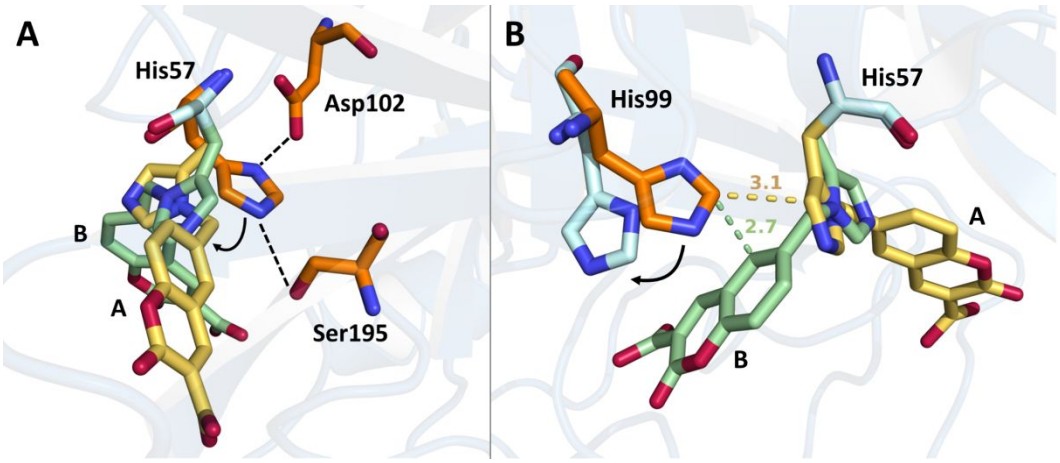

Figure 5. **Amino acid movements upon inhibitor binding.** The crystal structures of unliganded KLK7 (orange) and the complex with compound **2** (cyan or yellow/green for the two alternative inhibitor conformations, PDB code 6SHI) were superimposed based on the Cα atoms. (A) Side view of His57, Asp102 and Ser195 before and after inhibitor binding. (B) Front view showing the conformational change of His99.

The electron density maps further indicate that the ester linkage to the halophenyl moiety (exocyclic ester bond) of both inhibitor conformations is at least partially cleaved in all three structures (compound **1**, **2** and **3**). This is obvious for inhibitor conformation A, for which no space is available for the halophenyl moiety in the crystal lattice. In conformation B, more space is available but due to the half occupancy of the alternative conformation and possible additional flexibility, the electron density map does not clearly indicate the absence or presence of the substituent. We collected anomalous data at wavelength of 0.920172 Å to identify bromine in compound **2**. The absorption edge of bromine was detected at 0.9206 Å in a fluorescence scan, but no distinct strong maximum ("white line") after the edge was observed. For compound **3**, a wavelength of 2.101 Å (at the high energy side of the iodine L_I absorption edge, expected at 2.3898 Å) was used to locate potential iodine positions. However, the anomalous density maps also revealed no binding sites of these halogens.

Inhibited KLK7 was crystallized in HEPES buffer at pH 8.5 containing 2.9 M ammonium sulphate. To assure that hydrolysis of the exocyclic ester bond is not an artefact of the crystallization process, we analyzed

the protease inhibited by compound **2** prior to crystallization by mass spectrometry and compared the spectrum with unliganded KLK7. Analysis of a tryptic digestion of unliganded KLK7 showed the peptide of interest ($WVLTAAH_{57}CK$) with a mass of 1085.5 Da. MS experiments after tryptic digestion of inhibited KLK7 revealed three additional peptide peaks (1445.62 Da, 1287.59 Da, 1243.59 Da), whereas the peak at 1085.5 Da is also detected in the inhibited KLK7 sample (Figure 6). We detected the mass of 1445.62 Da of compound **2** bound to the N_{δ}-atom of His57 after loss of the chlorine atom (calculated mass 1445.6 Da) and 1287.59 Da, the mass of the linked fragment observed in the crystal structure (calculated mass of 1287.6 Da). The third new signal at 1243.59 Da likely represents the peptide with the decarboxylated inhibitor fragment (calculated mass 1243.6 Da). Decarboxylation may result from the MS procedure. Thus, the exocyclic ester bond of the covalently bound inhibitor is at least partially cleaved prior to crystallization. Further, it is likely that the solution of inhibited KLK7 contains residual uninhibited KLK7 molecules giving a signal at 1085.5 Da in MS but do not crystallize later on, as the formation of the $P2_12_12_1$ crystal form probably depends on the modification of His57 for the formation of the dimeric pair with interacting active sites (Figure 4D, Figure S1).

To ensure inhibitor stability prior to incubation with KLK7 we collected ESI-MS and ^{1}H- NMR spectra of compound **2** after storage in 100 % DMSO at -20 °C for several months. These experiments verified that the inhibitor is stable under storage conditions (data not shown).

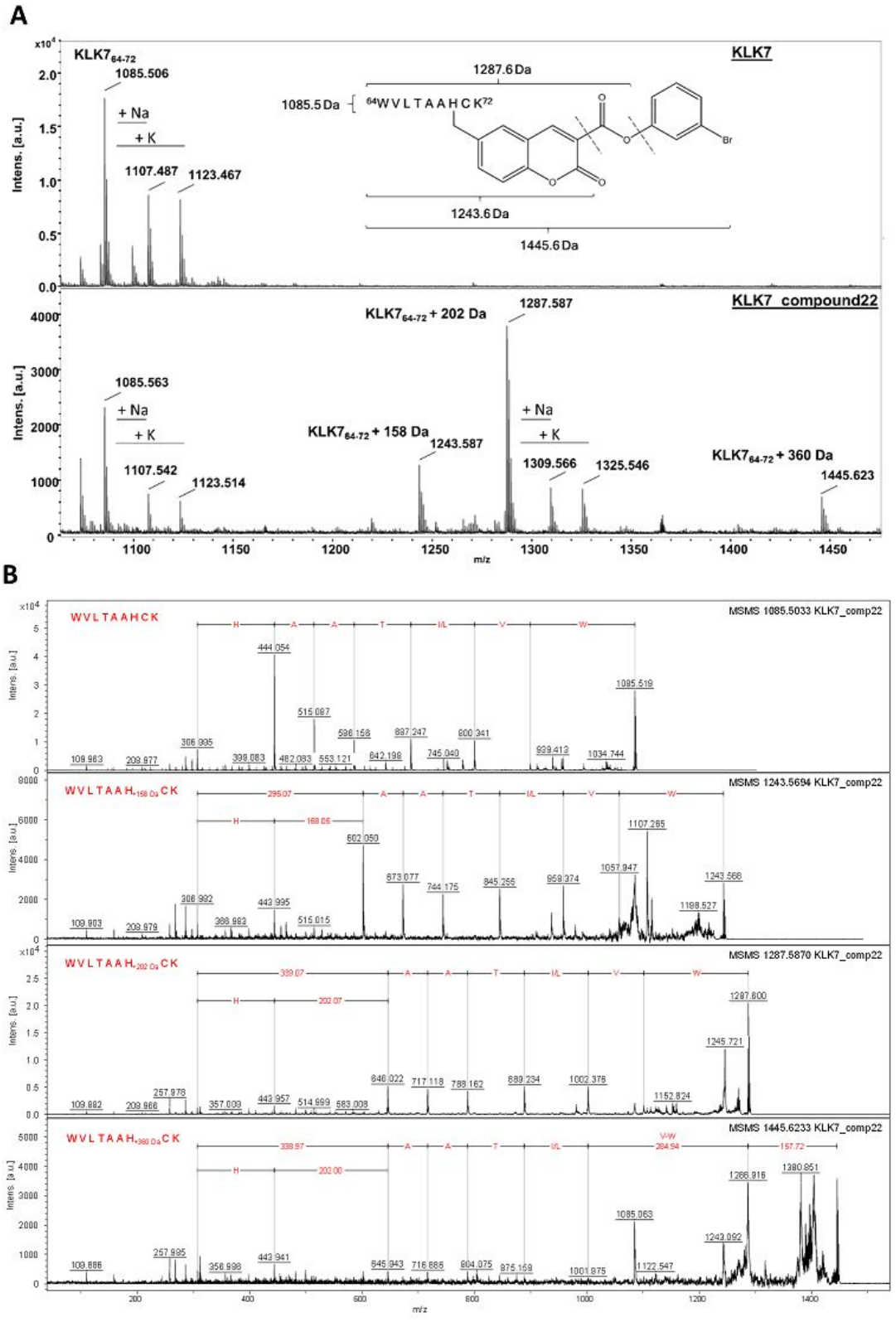

Figure 6. **MS and MS/MS spectra of native KLK7 and inhibited KLK7 by compound 2 after tryptic digestion.** (A) MS spectra of uninhibited KLK7 (upper spectrum) and the complex with compound **2** (lower spectrum). The latter spectrum shows three

additional peaks compared to unliganded KLK7 indicating a mass gain at His57. The mass gain results from covalent binding of compound **2** to His57. (B) MS/MS spectra of the three additional peaks in KLK7-compound **2**-complex revealed that the mass gains at His57 resulted from two inhibitor fragments and the attached uncleaved compound **2**. The native amino acid sequence of the peptide containing His57 would be WVLTAAH.

Modelling studies on the bridged intermediate and the final inhibited state. The crystal structures clearly show that the inhibitor is attached only to the N_δ-atom of His57. All information concerning the constitution of the inhibitor intermediate bridging His57 and Ser195 (Figure 7) is thus known and we modeled possible conformations of this intermediate state by a conformational search. In this calculation, the two amino acid residues and the bridging inhibitor were part of the conformational search whereas the rest of the protein was fixed. The resulting conformations showed that the bridge is sterically possible without very rare high energy torsion angles or other distortions, but several torsion angles have medium strain (Figure S2). This may be relieved by allowing for more flexibility of the rest of the protein in the conformational search, but it thus appears likely that the intermediate is strained favoring hydrolysis of the ester bond to Ser195 to relieve this strain. Modelling also explains why the inhibitor is not attached to the N_ε-atom of His57. In the conformation of His57 observed in the unliganded structure (His57 being part of the catalytic triad), the His57 side chain is close to the Ser195 side chain but not positioned to attack the quinone methide. In the alternative His57 side chain conformation observed in the inhibited state (Figure 4A) only the N_δ-atom is positioned close enough for the nucleophilic attack, whereas N_ε is not (in both conformations generated by a side chain flip of the imidazole group).

In the crystal structures, the inhibitors are covalently attached to His57 and present in two alternative conformations, each with about half occupancy (Figures 4 and 5). As the inhibitor conformations may be influenced by crystal packing contacts (Figure 4D), we investigated the stability of these conformations by torsion angle analysis (Figure S3) and molecular dynamics (MD) simulations (Figures S5-S8). Four free torsion angles determine the possible rotamers of the His57-inhibitor moiety. Both alternative conformations of the crystal structures have torsion angles that are frequently observed values or at least do

not correspond to rare high-energy torsion angles. In the MD simulations, rotamer A is stable, but the torsion angles change such that the coumarinic scaffold is positioned to form less contacts with the protein surface (Figures S5 and S6). Starting from rotamer B, another stable rotamer is predominantly observed in the simulations, in which torsion angles 3 and 4 (refer to Figure S5 for definition) adopt other minima such that the carboxylate group of the inhibitor forms a salt bridge with Arg90 (Figure S8). Taken together, these results indicate that the His57-inhibitor moiety can adopt several low energy conformations and the final inhibitory state should not pose strong restrictions on the substitution pattern of the coumarinic acid inhibitors due to this flexibility.

Comparison to known KLK7-inhibitor complex structures. Crystal structures have been previously determined for KLK7 in complex with peptide derivatives as well as non-peptidic synthetic inhibitors (Figure S9)[29,32,35,30,36,31,37]. All of these inhibitors employ the deep S1 pocket for binding using predominantly planar aromatic hydrophobic substituents. Also the 3-halophenyl substituent of **1-3** likely binds to this pocket in the initial binding mode with the halogen atom at the bottom of the pocket[33], similar to the binding of the 3-chlorophenyl group of the 1,4-diazepane-7-one compound shown in Figure S9C. Many inhibitors also bind to the S2, S1' and S2' binding sites or position a carbonyl group for interaction with the oxyanion hole. The peptide chloromethylketone inhibitors form covalent complexes with Ser195 and His57 (Fig. S9D), as the coumarinic inhibitors, but His57 maintains its conformation in the catalytic triad.

Discussion and Conclusions

Here we examined the binding of aromatic coumarinic esters as selective suicide inhibitors for KLK7. We focused on the aromatic esters of 6-chloromethylcoumarin-3-carboxylic acid **1-3** carrying chloride as leaving group at position 6, which do not display inhibition of the related enzymes KLK5, KLK14 and matriptase. The halomethyl moiety in 6-position is required to lead to an irreversible inhibition through covalent attachment at His57 of the catalytic triad[26].

It has been proposed, that the inhibitory mechanism of 6-chloromethylcoumarin-3-carboxylic acid compounds is initiated by nucleophilic attack of the catalytic Ser195 while opening the lactone ring (Figure 7)[27,25,26]. The covalent acyl-enzyme intermediate is thought to promote expulsion of the chloride ion at the chloromethyl substituent, leading to the formation of a quinone methide, which is susceptible to nucleophilic attack by His57 of the catalytic triad[26].

In our X-ray crystallographic studies, we observed the protease in a state, in which the inhibitors are covalently attached only to His57. Susceptibility of the ester linkage to Ser195 for cleavage has been noted previously[38]. In fact, the inhibitory potency of the coumarinic esters strongly depends on the alkylating character of the substituent in the 6-position[26]. Without this function, the inhibitors act transiently due to hydrolysis of the ester linkage between the serine nucleophile and the inhibitor. However, even in the presence of alkylating functions in the 6-position, the nature of the inhibition mechanism (transient vs. permanent) and the overall inhibitory potency do not only depend on the strength of the alkylating character of the 6-substituent but also on the 3-substituent and the type of the inhibited enzyme.

Mechanistic and structural differences between enzymes have been found for chymotrypsin compared to human leukocyte elastase[24,27,25] and also between kallikrein-related peptidases 5, 7, 14 and matriptase[26]. The efficiency of the alkylation step likely depends primarily on the ability of the His side chain and the Ser-linked quinone methide to adopt energetically favorable conformations that are productive for the presumed nucleophilic attack of the His N_{δ}-atom on the C=C bond of the quinone methide. The observed influence of substitutions at the 3-position on the alkylation step might be caused by destabilization of productive conformations of the quinone methide or by stabilizing alternative non-productive conformations.

In addition, the enzyme environment can influence the conformational flexibility of the two reacting side chains. As an example, we compare the environment of the His nucleophile in the catalytically productive conformation of KLK7 and matriptase in Figure S4. The environment of the His side chain in matriptase is much more restricted by Phe99 and Ile60 compared to the situation in KLK7[39]. This might influence the initial binding mode of the inhibitors prior to attack of Ser195 and the efficiency for alkylation of His57.

However, also differences in protein dynamics influenced by more remote structural variations can influence the inhibition kinetics. More detailed computational studies by conformational search calculations, molecular dynamics simulations and energy ranking algorithms might be employed based on available structural information to rationalize available structure-activity relationships for various enzymes and to aid further inhibitor development by structure-based methods.

Ester bond cleavage of the Ser195 might be promoted through steric strain of the covalent intermediate in which Ser195 and His57 are bridged by the inhibitor (Figure 7, Figure S3). After cleavage of the ester bond to Ser195, the equilibrium between the free carboxylate group and the lactone favors the ester formation. Interestingly, also the exocyclic ester bond to the halogenated phenyl substituent was hydrolyzed after binding of the compound to the protein and before crystallization. The remaining aromatic part of the inhibitor is present in two alternative conformations (Figure 4). For conformation A the electron density clearly indicates the cleaved inhibitor. This hydrolysis may as well be promoted by basic conditions. Although the substituent is thus not required for the final inhibitory state of KLK7, previous studies showed that its presence is essential for substrate specificity. Derivatives with unsubstituted phenyl ester groups had only low inhibitory effects on KLK7[26]. The initial inhibitory binding mode determining substrate specificity has been modeled previously[26,33]. As discussed above, the inhibitor specificity is determined not only by the initial inhibitor binding mode leading to Ser195 attack, but also by the efficiency of the following steps for His57 alkylation. Inhibitors that form the acyl-enzyme intermediate to Ser195, but cannot be efficiently transferred to His57, are only transient inhibitors, as the covalent bond to His57 after alkylation is more stable than the ester bond to Ser195. The observation of two alternative conformations of the final inhibited state and possible further conformational freedom indicated by the MD simulations strongly suggests that the stability of this state is not influenced by substituents of the coumarinic ester scaffold as long as the chemical stability of the alkylated His57 is not affected. In contrast, substituents likely influence the inhibitor selectivity via the initial non-covalent binding mode and the efficiency of the transfer step to His57.

Based on these findings two ester hydrolysis steps may likely occur after incubation of compounds **1**, **2** or **3** with KLK7 and before crystallization (Figure 7). However, on the basis of the available data it is not possible to conclude if the ester bonds are hydrolyzed independently of each other. An alternative to the mechanism depicted in Figure 7 is that Ser195 forms an acyl intermediate via the exocyclic ester bond. This possibility appears less likely to us as a reactive quinone methide would not form and a direct attack of the Cl-CH_2 carbon with expulsion of the chloride ion is chemically less probable[40,41].

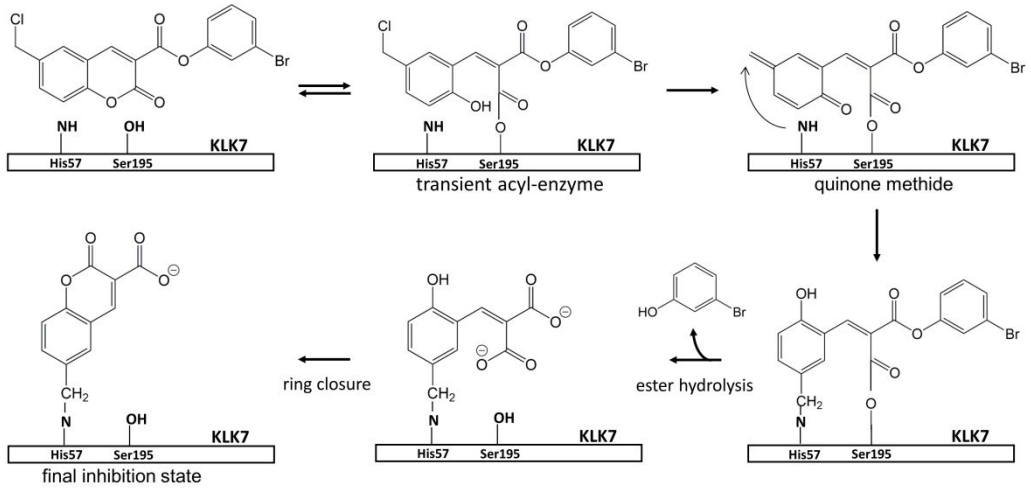

Figure 7. **Model for the reaction mechanism of aromatic coumarinic esters with KLK7.** The initial steps are as described by Tan *et al.* 2015. Nucleophilic attack of Ser195 results in opening of the lactone ring and a covalent acyl-enzyme intermediate is formed. After expulsion of the chloride ion, a quinone methide may be formed as an intermediate. Nucleophilic attack on the quinone methide by His57 results in a structure in which the inhibitor is covalently attached to His57 and Ser195. The ester bond to Ser195 undergoes hydrolysis and the lactone ring is formed again. In addition, the ester bond to the halophenyl moiety is hydrolyzed.

In conclusion, we co-crystallized the serine protease KLK7 together with three aromatic coumarinic esters, which irreversibly inhibit the protease in the nM range. Their structures were determined by X-ray crystallography to resolutions between 1.85 Å and 2.02 Å. In these structures, 6-methylcoumarin-3-carboxylate bound covalently to the N_δ-atom of His57 of the KLK7 active site in two alternative conformations and MD simulations indicate a further low energy conformation. Thus, the final inhibited state does not pose significant restraints on the choice substituents and the substituents need not to

be optimized for specific interactions with proteins surface. The core coumarinic scaffold is large enough to ensure that His57 swings out of its catalytically competent conformation in the catalytic triad upon alkylation. Instead, the substituents need to provide selectivity for initial binding to the target enzyme in a position for catalytic attack of the Ser195 nucleophile on the lactone bond. In addition, the substituents need to support an efficient transfer to His57, such that they allow for a rearrangement of the inhibitor for attack of the His57 nucleophile. The crystal structures of the inactivated enzyme give new information about the unexplored steps of enzyme alkylation that follow the non-covalent binding of the inhibitor to the enzyme and the Ser195 acylation. The obtained structures show that Ser195 is only transiently acylated during the reaction. Finally, these results help to characterize the covalent inhibition mechanism of this inhibitor class, in particular to rationalize the structural factors that govern the efficiency of covalent inhibition, which dominates the overall potency of this inhibitor class of serine proteases.

Experimental Section

Protein Expression and Purification. The mature wild type protease KLK7 was expressed in *E. coli* Rosetta (DE3) pLysS cells. Therefore, residues I30- R253 were fused to an N-terminal SUMO- and His_6-tag provided by the vector pET-SUMO. The protein accumulated in inclusion bodies and was refolded and purified as described in detail elsewhere. Briefly, the cells were disrupted with a FastPrep-24^{TM}5G cell homogenizer (MP Biomedicals) and the inclusion bodies were purified as published previously[42]. The inclusion bodies were solubilized in 6 M guanidin-HCl and 0.1 M Tris- HCl at pH 8.0. The unfolded fusion protein was purified by an immobilized metal ion affinity chromatography (IMAC) using NiSepharose 6 Fast Flow resin (GE Healthcare). After reducing the protein with 100 mM DTT, the buffer was exchanged stepwise to 3 M guanidin- HCl and 0.01 M Tris- HCl, pH 8.0. Refolding was performed by fast dilution at 4 °C into a buffer containing 0.7 M arginine- HCl, 10 % glycerol and 1 mM EDTA at pH 8.0. After 5 days at 19 °C the refolded protein was concentrated and the buffer was exchanged through dialysis to 0.05 M Tris-HCl, pH 8.0, and 0.15 M NaCl before the fusion-tag was cut off with the SUMO protease. The resulting

protein fragments were separated by a combined IMAC and cation exchange chromatography (GE Healthcare). After size exclusion chromatography a final affinity chromatography with immobilized SBTI (soybean trypsin inhibitor) (Oxford Biomedical Research) was performed to separate active from inactive KLK7. Purified KLK7 was stored at -80 °C in 50 mM sodium phosphate buffer, pH 7.5 with a protein concentration of 5 mg/mL.

Thermal stability. To determine the thermal stability of active and inhibited KLK7, differential scanning fluorimetry (DSF) was performed, using a Prometheus NT.48 instrument (NanoTemper Technologies GmbH). 10 µL of 1 mg/mL KLK7 solution were loaded into nanoDSF grade standard capillaries (NanoTemper) and the unfolding ramp was measured from 20 °C to 95 °C with 1 °C/min. The intrinsic fluorescence of tryptophan and tyrosine residues was detected at 330 nm and 350 nm to determine the unfolding state of the protein from the changes in the F350/F330 fluorescence ratio. We determined the T_m values in a buffer of 50 mM sodium phosphate, pH 7.5 and increasing DMSO concentrations.

Activity measurements. Activity of the purified protease was determined with the fluorogenic peptide substrate NFF-3 [Mca-RPKPVE-Nva-WR-K(Dnp)-NH_2, where Mca is (7-methoxycoumarin-4-yl) acetyl, Nva is norvaline, and Dnp is 2,4-dinitrophenyl] (AnaSpec) using a protocol from R&D Systems with minor modifications. Briefly, 50 ng KLK7 were incubated with 42 µM NFF-3 in protein buffer. The time-dependent increase of the fluorescence signal, resulting from cleavage of an amide bond between the fluorescent group (Mca) and the quencher group (Dnp), was recorded with a FlexStation microplate reader at excitation and emission wavelength of 320 nm and 405 nm, respectively.

For the vaspin inhibition assay, KLK7-inhibitor complexes were prepared as described below for the structural studies and concentrated with a 5 kDa spin column. KLK7-inhibitor complexes were mixed with vaspin in a molar ratio of 3:1 as described before[19]. Therefore, 3.15 µM KLK7 was mixed with 1.05 µM vaspin in 50 mM Tris, 150 mM NaCl, pH 8.0 and was incubated at room temperature. At given time points, samples were taken, mixed with an appropriate amount of reducing SDS buffer and incubated for 5 min at

95 °C. The samples were loaded onto 12 % polyacrylamide gels and stained with Coomassie blue after gel electrophoresis.

Crystallization, data collection and structure analysis. The compounds were synthesized as described before by Tan et al. 2015. The compounds were dissolved in 100 % DMSO to prepare stock solutions of 100 mM (compound **1** and **3**) or 25 mM (compound **2**), which were stored at -20 °C. Due to the low solubility of the compounds, KLK7 was incubated at low protein concentration. Therefore, the protease was diluted to a concentration of 0.123 mM in 50 mM sodium phosphate buffer, pH 7.5. The compounds were diluted to 10 mM in 100 % DMSO and added to the protein solution to achieve a concentration of 1 mM, resulting in a final DMSO concentration of 10 % (v/v). The reaction was incubated at 37 °C for 30 minutes and afterwards centrifuged for 10 minutes at 16.000xg to remove precipitate. For crystallization, the inhibited protease and the active protease was concentrated to 4.8 mg/mL and 3 mg/mL, respectively, using Vivaspin® 500 ultrafiltration spin columns (Sartorius, MWCO 5.000 Da). Crystallization was performed with the hanging drop vapor diffusion method. Drops were produced by mixing 0.5 µL of protein solution with 0.5 µL of crystallization buffer (2.9 M ammonium sulphate, 0.1 M HEPES, pH 8.5 and 0.5- 2 % PEG 3350). Crystallization trays for the inhibited protease were stored at 4 °C, crystals appeared after 10 days and grew to a size of 200 µm. Crystallization trays for native KLK7 were stored at 19 °C and crystals appeared overnight with a size of 200 µm. For cryo-protection, crystals were transferred into crystallization buffer containing 14 % (v/v) glycerol and directly flash frozen in liquid nitrogen. X-ray data collection took place at beamline 14.1 of the BESSY synchrotron Berlin with a Pilatus6M detector. Data reduction and scaling of images were performed with the program XDS[43]. Merging of reflexes was done with the program AIMLESS[44]. To obtain a good starting model for refinement, we superposed a high-resolution structure of KLK7 (PDB entry 2QXI[30] analyzed at 1.0 Å resolution) onto the KLK7 structure 3BSQ[28] (2.9 Å resolution), which has the same crystal form as our structure. In case of crystal form II (KLK7-inhibitor complex), the program PHASER[45] was used for molecular placement using 2QXI as the search model. The programs COOT[46], REFMAC5[47] and BUSTER[48] were used for model building and refinement. Stereochemical

restraints for the inhibitor were generated by the Grade Web Server[49]. Figure S2A shows a Polder omit map[50] of the bound ligand in chain A.

Molecular modelling and molecular dynamics simulations. The software MOE (Chemical Computing Group ULC, Montreal, Canada) was used for the conformational search to explore a model for the coumarinic inhibitor bridging Ser195 and His57. An initial model was manually build using the Molecular Builder based on the covalent complex structure determined in this work and energy minimized to relieve bond length and angle distortions. A conformational search was carried out for the complete amino acids 57 and 195 and the bridging inhibitor atoms. For MD simulations the programs MOE and NAMD[51] were used. Conformers A and B of chain A in the asymmetric unit of the structure 6SHI were used as the starting point. Water molecules were added to a drop with 25 Å radius around the His57-inhibitor atoms (MOE option Solvate). The structure was titrated and polar hydrogens were positioned (MOE option Solvate3D). Residues with at least one atom within a distance of 15 Å around the His57-inhibitor group were allowed to move freely. In a further shell of 3 Å distance the residues were tethered to their initial positions and all further atoms were fixed. The system was first energy minimized within MOE. For the simulations the software NAMD was used and the system was equilibrated first for 100 ps followed by a simulation of 20 ns. Five simulations were run for each of the two conformers as shown in Figures S5-S8. VMD[52] was used for analysis of the trajectories.

Complex formation of KLK7 with the serpin vaspin. Successful inhibition of KLK7 after compound incubation, was validated using its natural inhibitor vaspin. The latter forms a covalent complex with active KLK7[18]. Both proteins were incubated in 50 mM Tris pH 7.5, 150 mM NaCl for 60 minutes at room temperature. The samples were analyzed by a 12 % SDS-PAGE.

Mass spectrometry analysis of inhibited KLK7. MS and MS/MS experiments were performed to analyze the amino acid sequence of inhibited KLK7 and the apoprotein to determine the alkylated amino acid residues. For each experiment 1 µg of protein was digested with 100 ng Trypsin Gold (Promega, mass spectrometry grade) according to the manufacturers' protocol. Samples were desalted with C18-ZipTip filter

tips (Pierce) prior to analysis by MALDI-TOF MS and MS/MS using LIFT mode on a Bruker Ultraflex III MALDI TOF/TOF mass spectrometer. Peak lists of combined MS and MS/MS spectra were searched against the NCBIprot database using BioTools software (Bruker) and the Mascot search engine (Matrix Science, London, UK) to identify peptide fragments. The following parameters were used for database searches: species *homo sapiens*; enzyme – trypsin; monoisotopic masses; optional modifications – methionine oxidation, cysteine alkylation (iodoacetamide); mass tolerance MS 150 ppm; mass tolerance MS/MS - 0.75 Da; maximum missed cleavage sites 2.

Ancillary Information

Supporting information

Additional figures illustrating crystal packing, superpositions and modelling results.

Accession Codes

PDB codes for the co-crystal structures with compounds **1**, **2** and **3** are 6SHH, 6SHI and 6SJU, respectively, and 6Y4S for unliganded KLK7. Authors will release the atomic coordinates and experimental data upon article publication.

Corresponding Author Information

*Email: strater@bbz.uni-leipzig.de

Author Contributions

SH designed and conducted experiments and analyzed data. SH and JP expressed and purified KLK7. CAT and DU expressed and purified vaspin. JTH performed MS analysis. MR evaluated and BP synthesized the inhibitory compounds. SH wrote the initial draft of the manuscript. All authors contributed to data interpretation and manuscript preparation. JTH and NS supervised the project.

Acknowledgements

The authors thank PD Dr. Jürgen Schiller for ^{1}H-NMR and Dr. Yulia Popkova for ESI-MS measurements, as well as Dr. Renato Weiße for support in X-ray data analysis. This work was supported by grants of the Collaborative Research Centre "Obesity Mechanisms" SFB 1052 (C4 Sträter, C7 Heiker, Z4 Schiller). The authors thank the Joint Berlin MX-Laboratory (BESSY II, Helmholtz-Zentrum Berlin, Germany) and EMBL Hamburg at the PETRA III storage ring (DESY, Hamburg, Germany) for beam time, assistance during synchrotron data collection as well as for travelling support.

Abbreviations

KLK7 – human kallikrein-related peptidase 7, DSF – differential scanning fluorimetry, MWCO – molecular weight cutoff

References

(1) Egelrud, T. Purification and Preliminary Characterization of Stratum Corneum Chymotryptic Enzyme: A Proteinase That May Be Involved in Desquamation, *The Journal of investigative dermatology.* **1993**, *101,* pp. 200–204.

(2) Prassas, I.; Eissa, A.; Poda, G.; Diamandis, E. P. Unleashing the therapeutic potential of human kallikrein-related serine proteases, *Nat Rev Drug Discov.* **2015**, *14,* pp. 183–202.

(3) Kalinska, M.; Meyer-Hoffert, U.; Kantyka, T.; Potempa, J. Kallikreins – The melting pot of activity and function, *Biochimie.* **2016**, *122,* pp. 270–282.

(4) Sondell, B.; Thornell, L. E.; Egelrud, T. Evidence that stratum corneum chymotryptic enzyme is transported to the stratum corneum extracellular space via lamellar bodies, *The Journal of investigative dermatology.* **1995**, *104,* pp. 819–823.

(5) Ishida-Yamamoto, A.; Simon, M.; Kishibe, M.; Miyauchi, Y.; Takahashi, H.; Yoshida, S.; O'Brien, T. J.; Serre, G.; Iizuka, H. Epidermal lamellar granules transport different cargoes as distinct aggregates, *The Journal of investigative dermatology.* **2004**, *122,* pp. 1137–1144.

(6) Ishida-Yamamoto, A.; Deraison, C.; Bonnart, C.; Bitoun, E.; Robinson, R.; O'Brien, T. J.; Wakamatsu, K.; Ohtsubo, S.; Takahashi, H.; Hashimoto, Y.; Dopping-Hepenstal, P. J. C.; McGrath, J. A.; Iizuka, H.; Richard, G.; Hovnanian, A. LEKTI is localized in lamellar granules, separated from KLK5 and KLK7, and is secreted in the extracellular spaces of the superficial stratum granulosum, *The Journal of investigative dermatology.* **2005**, *124,* pp. 360–366.

(7) Ekholm, I. E.; Brattsand, M.; Egelrud, T. Stratum corneum tryptic enzyme in normal epidermis: a missing link in the desquamation process?, *The Journal of investigative dermatology.* **2000**, *114,* pp. 56–63.

(8) Caubet, C.; Jonca, N.; Brattsand, M.; Guerrin, M.; Bernard, D.; Schmidt, R.; Egelrud, T.; Simon, M.; Serre, G. Degradation of corneodesmosome proteins by two serine proteases of the kallikrein family, SCTE/KLK5/hK5 and SCCE/KLK7/hK7, *The Journal of investigative dermatology.* **2004**, *122,* pp. 1235–1244.

(9) Borgoño, C. A.; Michael, I. P.; Komatsu, N.; Jayakumar, A.; Kapadia, R.; Clayman, G. L.; Sotiropoulou, G.; Diamandis, E. P. A potential role for multiple tissue kallikrein serine proteases in epidermal desquamation, *The Journal of biological chemistry.* **2007**, *282,* pp. 3640–3652.

(10) Simon, M.; Jonca, N.; Guerrin, M.; Haftek, M.; Bernard, D.; Caubet, C.; Egelrud, T.; Schmidt, R.; Serre, G. Refined characterization of corneodesmosin proteolysis during terminal differentiation of human epidermis and its relationship to desquamation, *The Journal of biological chemistry.* **2001**, *276,* pp. 20292–20299.

(11) Descargues, P.; Deraison, C.; Prost, C.; Fraitag, S.; Mazereeuw-Hautier, J.; D'Alessio, M.; Ishida-Yamamoto, A.; Bodemer, C.; Zambruno, G.; Hovnanian, A. Corneodesmosomal cadherins are preferential targets of stratum corneum trypsin- and chymotrypsin-like hyperactivity in Netherton syndrome, *The Journal of investigative dermatology.* **2006**, *126,* pp. 1622–1632.

(12) Morizane, S.; Yamasaki, K.; Kajita, A.; Ikeda, K.; Zhan, M.; Aoyama, Y.; Gallo, R. L.; Iwatsuki, K. TH2 cytokines increase kallikrein 7 expression and function in patients with atopic dermatitis, *The Journal of allergy and clinical immunology.* **2012**, *130,* 259-61.e1.

(13) Borgoño, C. A.; Diamandis, E. P. The emerging roles of human tissue kallikreins in cancer, *Nature reviews. Cancer.* **2004**, *4,* pp. 876–890.

(14) Ramani, V. C.; Hennings, L.; Haun, R. S. Desmoglein 2 is a substrate of kallikrein 7 in pancreatic cancer, *BMC cancer.* **2008**, *8,* p. 373.

(15) Haddada, M.; Draoui, H.; Deschamps, L.; Walker, F.; Delaunay, T.; Brattsand, M.; Magdolen, V.; Darmoul, D. Kallikrein-related peptidase 7 overexpression in melanoma cells modulates cell adhesion leading to a malignant phenotype, *Biological chemistry.* **2018**, *399,* pp. 1099–1105.

(16) Zieger, K.; Weiner, J.; Kunath, A.; Gericke, M.; Krause, K.; Kern, M.; Stumvoll, M.; Klöting, N.; Blüher, M.; Heiker, J. T. Ablation of kallikrein 7 (KLK7) in adipose tissue ameliorates metabolic consequences of high fat diet-induced obesity by counteracting adipose tissue inflammation in vivo, *Cellular and molecular life sciences : CMLS.* **2018**, *75,* pp. 727–742.

(17) Debela, M.; Magdolen, V.; Schechter, N.; Valachova, M.; Lottspeich, F.; Craik, C. S.; Choe, Y.; Bode, W.; Goettig, P. Specificity profiling of seven human tissue kallikreins reveals individual subsite preferences, *The Journal of biological chemistry.* **2006**, *281,* pp. 25678–25688.

(18) Heiker, J. T.; Klöting, N.; Kovacs, P.; Kuettner, E. B.; Sträter, N.; Schultz, S.; Kern, M.; Stumvoll, M.; Blüher, M.; Beck-Sickinger, A. G. Vaspin inhibits kallikrein 7 by serpin mechanism, *Cellular and molecular life sciences : CMLS.* **2013**, *70,* pp. 2569–2583.

(19) Ulbricht, D.; Pippel, J.; Schultz, S.; Meier, R.; Sträter, N.; Heiker, J. T. A unique serpin P1' glutamate and a conserved β-sheet C arginine are key residues for activity, protease recognition and stability of serpinA12 (vaspin), *The Biochemical journal.* **2015**, *470,* pp. 357–367.

(20) Schechter, N. M.; Choi, E.-J.; Wang, Z.-M.; Hanakawa, Y.; Stanley, J. R.; Kang, Y.'a.; Clayman, G. L.; Jayakumar, A. Inhibition of human kallikreins 5 and 7 by the serine protease inhibitor lympho-epithelial Kazal-type inhibitor (LEKTI), *Biological chemistry.* **2005**, *386,* pp. 1173–1184.

(21) Krastel, P.; Liechty, B.-M.; Schmitt, E.; Schreiner, E. P. (2013) Use of cyclic depsipeptides to inhibit kallikrein 7. United States Patent Application 20130172267.

(22) Veer, S. J. de; Furio, L.; Swedberg, J. E.; Munro, C. A.; Brattsand, M.; Clements, J. A.; Hovnanian, A.; Harris, J. M. Selective Substrates and Inhibitors for Kallikrein-Related Peptidase 7 (KLK7) Shed Light on KLK Proteolytic Activity in the Stratum Corneum, *The Journal of investigative dermatology.* **2017**, *137,* pp. 430–439.

(23) Masurier, N.; Arama, D. P.; El Amri, C.; Lisowski, V. Inhibitors of kallikrein-related peptidases: An overview, *Medicinal research reviews.* **2018**, *38,* pp. 655–683.

(24) Pochet, L.; Doucet, C.; Schynts, M.; Thierry, N.; Boggetto, N.; Pirotte, B.; Jiang, K. Y.; Masereel, B.; Tullio, P. de; Delarge, J.; Reboud-Ravaux, M. Esters and amides of 6-(chloromethyl)-2-oxo-2H-1-benzopyran-3-carboxylic acid as inhibitors of alpha-chymotrypsin: significance of the "aromatic" nature of the novel ester-type coumarin for strong inhibitory activity, *Journal of Medicinal Chemistry.* **1996**, *39,* pp. 2579–2585.

(25) Pochet, L.; Doucet, C.; Dive, G.; Wouters, J.; Masereel, B.; Reboud-Ravaux, M.; Pirotte, B. Coumarinic derivatives as mechanism-based inhibitors of alpha-chymotrypsin and human leukocyte elastase, *Bioorganic & medicinal chemistry.* **2000**, *8,* pp. 1489–1501.

(26) Tan, X.; Soualmia, F.; Furio, L.; Renard, J.-F.; Kempen, I.; Qin, L.; Pagano, M.; Pirotte, B.; El Amri, C.; Hovnanian, A.; Reboud-Ravaux, M. Toward the first class of suicide inhibitors of kallikreins involved in skin diseases, *Journal of Medicinal Chemistry.* **2015**, *58,* pp. 598–612.

(27) Doucet, C.; Pochet, L.; Thierry, N.; Pirotte, B.; Delarge, J.; Reboud-Ravaux, M. 6-Substituted 2-Oxo-2 H -1-benzopyran-3-carboxylic Acid as a Core Structure for Specific Inhibitors of Human Leukocyte Elastase †, *Journal of Medicinal Chemistry.* **1999**, *42,* pp. 4161–4171.

(28) Fernández, I. S.; Ständker, L.; Mägert, H.-J.; Forssmann, W.-G.; Giménez-Gallego, G.; Romero, A. Crystal structure of human epidermal kallikrein 7 (hK7) synthesized directly in its native state in E. coli: insights into the atomic basis of its inhibition by LEKTI domain 6 (LD6), *Journal of molecular biology.* **2008**, *377,* pp. 1488–1497.

(29) Murafuji, H.; Sakai, H.; Goto, M.; Imajo, S.; Sugawara, H.; Muto, T. Discovery and structure-activity relationship study of 1,3,6-trisubstituted 1,4-diazepane-7-ones as novel human kallikrein 7 inhibitors, *Bioorganic & medicinal chemistry letters.* **2017**, *27,* pp. 5272–5276.

(30) Debela, M.; Hess, P.; Magdolen, V.; Schechter, N. M.; Steiner, T.; Huber, R.; Bode, W.; Goettig, P. Chymotryptic specificity determinants in the 1.0 A structure of the zinc-inhibited human tissue kallikrein 7, *Proceedings of the National Academy of Sciences of the United States of America.* **2007**, *104,* pp. 16086–16091.

(31) Maibaum, J.; Liao, S.-M.; Vulpetti, A.; Ostermann, N.; Randl, S.; Rüdisser, S.; Lorthiois, E.; Erbel, P.; Kinzel, B.; Kolb, F. A.; Barbieri, S.; Wagner, J.; Durand, C.; Fettis, K.; Dussauge, S.; Hughes, N.; Delgado, O.; Hommel, U.; Gould, T.; Mac Sweeney, A.; Gerhartz, B.; Cumin, F.; Flohr, S.; Schubart, A.; Jaffee, B.;

Harrison, R.; Risitano, A. M.; Eder, J.; Anderson, K. Small-molecule factor D inhibitors targeting the alternative complement pathway, *Nature chemical biology.* **2016**, *12,* pp. 1105–1110.

(32) Murafuji, H.; Muto, T.; Goto, M.; Imajo, S.; Sugawara, H.; Oyama, Y.; Minamitsuji, Y.; Miyazaki, S.; Murai, K.; Fujioka, H. Discovery and structure-activity relationship of imidazolinylindole derivatives as kallikrein 7 inhibitors, *Bioorganic & medicinal chemistry letters.* **2019**, *29,* pp. 334–338.

(33) Zheng, X.; He, M.; Tan, X.; Zheng, J.; Wang, F.; Liu, S. 3D-quantitative structure-activity relationship and docking studies of coumarin derivatives as tissue kallikrein 7 inhibitors, *The Journal of pharmacy and pharmacology.* **2017**, *69,* pp. 1136–1144.

(34) Buller, A. R.; Townsend, C. A. Intrinsic evolutionary constraints on protease structure, enzyme acylation, and the identity of the catalytic triad, *Proceedings of the National Academy of Sciences of the United States of America.* **2013**, *110,* E653-61.

(35) Murafuji, H.; Sugawara, H.; Goto, M.; Oyama, Y.; Sakai, H.; Imajo, S.; Tomoo, T.; Muto, T. Structure-based drug design to overcome species differences in kallikrein 7 inhibition of 1,3,6-trisubstituted 1,4-diazepan-7-ones, *Bioorganic & medicinal chemistry.* **2018**, *26,* pp. 3639–3653.

(36) Debela, M.; Beaufort, N.; Magdolen, V.; Schechter, N. M.; Craik, C. S.; Schmitt, M.; Bode, W.; Goettig, P. Structures and specificity of the human kallikrein-related peptidases KLK 4, 5, 6, and 7, *Biological chemistry.* **2008**, *389,* pp. 623–632.

(37) Murafuji, H.; Sakai, H.; Goto, M.; Oyama, Y.; Imajo, S.; Sugawara, H.; Tomoo, T.; Muto, T. Structure-based drug design of 1,3,6-trisubstituted 1,4-diazepan-7-ones as selective human kallikrein 7 inhibitors, *Bioorganic & medicinal chemistry letters.* **2018**, *28,* pp. 1371–1375.

(38) Reboud-Ravaux, M.; Desvages, G.; Chapeville, F. Irreversible inhibition and peptide mapping of urinary plasminogen activator urokinase, *FEBS Letters.* **1982**, *140,* pp. 58–62.

(39) Friedrich, R.; Fuentes-Prior, P.; Ong, E.; Coombs, G.; Hunter, M.; Oehler, R.; Pierson, D.; Gonzalez, R.; Huber, R.; Bode, W.; Madison, E. L. Catalytic domain structures of MT-SP1/matriptase, a matrix-degrading transmembrane serine proteinase, *The Journal of biological chemistry.* **2002**, *277,* pp. 2160–2168.

(40) Reboud-Ravaux, M.; Wakselman, M. Quinone Methides and Aza-Quinone Methides as Latent Alkylating Species in the Design of Mechanism-Based Inhibitors of Serine Proteases andβ-Lactamases. In *Quinone Methides;* Rokita, S. E., Ed.; John Wiley & Sons, Inc: Hoboken, NJ, USA, 2009, pp. 357–383.

(41) Toteva, M. M.; Richard, J. P. The Generation and Reactions of Quinone Methides, *Advances in physical organic chemistry.* **2011**, *45,* pp. 39–91.

(42) Rudolph, R.; Lilie, H. In vitro folding of inclusion body proteins, *FASEB journal : official publication of the Federation of American Societies for Experimental Biology.* **1996**, *10,* pp. 49–56.

(43) Kabsch, W. Automatic processing of rotation diffraction data from crystals of initially unknown symmetry and cell constants, *Journal of Applied Crystallography.* **1993**, *26,* pp. 795–800.

(44) Evans, P. R.; Murshudov, G. N. How good are my data and what is the resolution?, *Acta crystallographica. Section D, Biological crystallography.* **2013**, *69,* pp. 1204–1214.

(45) McCoy, A. J.; Grosse-Kunstleve, R. W.; Adams, P. D.; Winn, M. D.; Storoni, L. C.; Read, R. J. Phaser crystallographic software, *Journal of Applied Crystallography.* **2007**, *40,* pp. 658–674.

(46) Emsley, P.; Cowtan, K. Coot: model-building tools for molecular graphics, *Acta crystallographica. Section D, Biological crystallography.* **2004**, *60,* pp. 2126–2132.

(47) Murshudov, G. N.; Vagin, A. A.; Dodson, E. J. Refinement of macromolecular structures by the maximum-likelihood method, *Acta crystallographica. Section D, Biological crystallography.* **1997**, *53,* pp. 240–255.

(48) Bricogne G.; Blanc E.; Brandl M.; Flensburg C.; Keller P.; Paciorek W.; Roversi P.; Sharff A.; Smart O.S.; Vonrhein C.; Womack T.O. BUSTER version 2.10.3. **2017**.

(49) Smart, O. S.; Womack, T. O.; Sharff, A.; Flensburg, C.; Keller, P.; Paciorek, W.; Vonrhein, C.; Bricogne, G. (2011) Grade, version 1.2.13; http://www.globalphasing.com.

(50) Liebschner, D.; Afonine, P. V.; Moriarty, N. W.; Poon, B. K.; Sobolev, O. V.; Terwilliger, T. C.; Adams, P. D. Polder maps: improving OMIT maps by excluding bulk solvent, *Acta crystallographica. Section D, Structural biology.* **2017**, *73,* pp. 148–157.

(51) Phillips, J. C.; Braun, R.; Wang, W.; Gumbart, J.; Tajkhorshid, E.; Villa, E.; Chipot, C.; Skeel, R. D.; Kalé, L.; Schulten, K. Scalable molecular dynamics with NAMD, *Journal of computational chemistry.* **2005**, *26,* pp. 1781–1802.

(52) Humphrey, W.; Dalke, A.; Schulten, K. VMD: Visual molecular dynamics, *Journal of molecular graphics.* **1996**, *14,* pp. 33–38.

Table 1. **Data collection and refinement statistics**

	KLK7 × compound 1	KLK7 × compound 2	KLK7 × compound 3	KLK7 unliganded
PDB code	6SHH	6SHI	6SJU	6Y4S
Data collection				
Beamline	BESSY BL 14.1	BESSY BL 14.1	BESSY BL 14.1	BESSY BL 14.1
Wavelength (Å)	0.9184	0.920172	2.101	0.9184
Space group	$P2_12_12_1$	$P2_12_12_1$	$P2_12_12_1$	H32
Cell dimensions				
a, b, c (Å)	60.6, 116.4, 291.0	60.6, 117.0, 291.3	60.7, 117.0, 291.2	113.2 113.2 326.1
Resolution range (Å)	48.49 – 2.0 (2.04 – 2.0)	47.08 – 1.85 (1.88 – 1.85)	47.08-2.20 (2.24-2.20)	48.45-2.23 (2.30-2.23)
Unique reflections	138687 (5745)	177629 (8592)	100395 (4514)	39789 (3526)
Completeness (%)	99.2 (84.1)	99.8 (98.7)	94.9 (87.2)	99.8 (97.6)
Multiplicity	9.4 (8.5)	7.4 (7.3)	12.6 (9.6)	15.0 (13.7)
$\langle I/\sigma(I)\rangle$	5.8 (0.5)	9.5 (1.1)	18.5 (3.0)	6.3 (0.5)
R_{meas}	0.369 (4.638)	0.169 (2.131)	0.095 (0.750)	0.452 (6.728)
R_{pim}	0.119 (1.536)	0.061 (0.772)	0.026 (0.235)	0.116 (1.792)
$CC_{1/2}$	0.993 (0.229)	0.997 (0.423)	0.999 (0.861)	0.994 (0.296)
Wilson B factor (Å^2)	31.6	21.0	32.0	40.5
Refinement				
Resolution range (Å)	47.03 – 2.0	46.6 – 1.85	47.08 – 2.20	48.45-2.23
R_{work} / R_{free} (%)	18.9 / 22.6	17.6 / 20.8	17.4 / 22.9	21.9 / 24.2
No. of atoms				
Protein	13429	13429	13429	5115
Solvent atoms	1180	1905	1465	82
Ligands, ions	685	705	740	80
Average B-factors (Å^2)				
Protein	41.1	30.6	39.0	55.9
Water	45.5	45.3	51.6	45.8
Ligands	73.6	59.6	63.6	90.4
R.m.s. deviation				
Bond length (Å^2)	0.012	0.013	0.010	0.008
Bond angles (°)	1.27	1.15	1.12	1.10
Ramachandran plot				
Favored region (%)	95.58	96.32	95.92	93.35
Allowed region (%)	4.37	3.62	3.96	4.5
Outlier region (%)	0.06	0.06	0.11	0.15

TOC

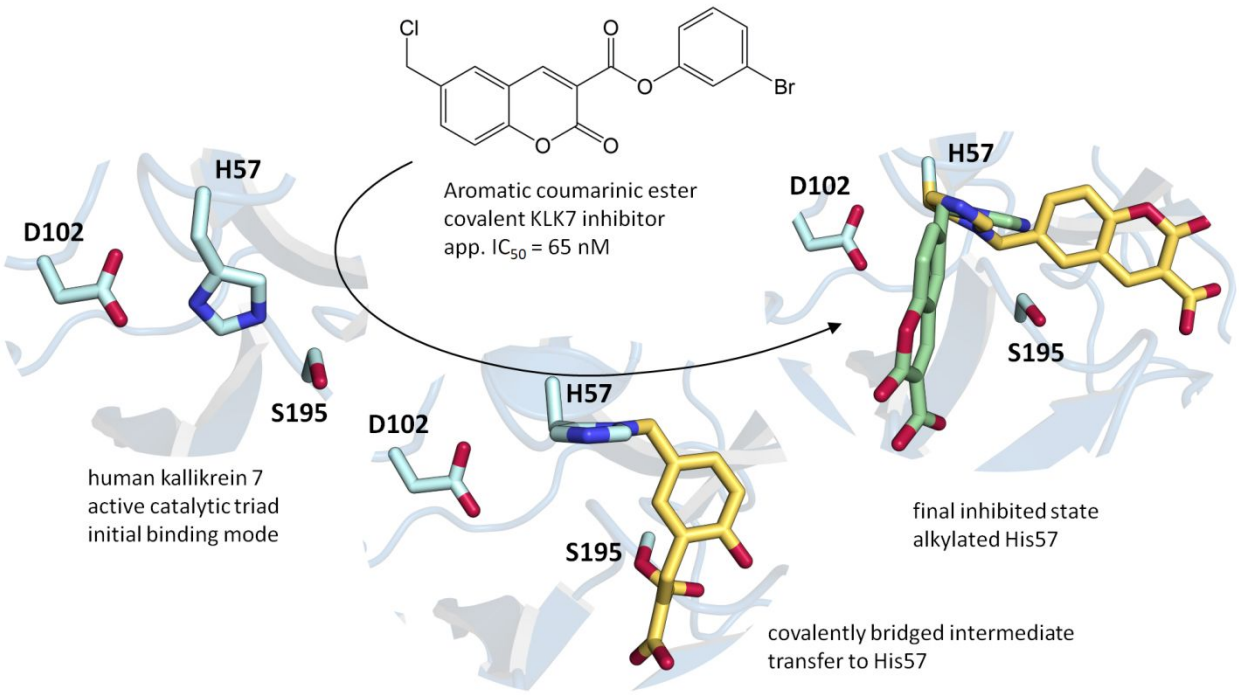
Cl
O
O
O
Br
O
Aromatic coumarinic ester
covalent KLK7 inhibitor
app. IC50 = 65 nM
H57
D102
S195
human kallikrein 7
active catalytic triad
initial binding mode
H57
D102
S195
covalently bridged intermediate
transfer to His57
H57
D102
S195
final inhibited state
alkylated His57

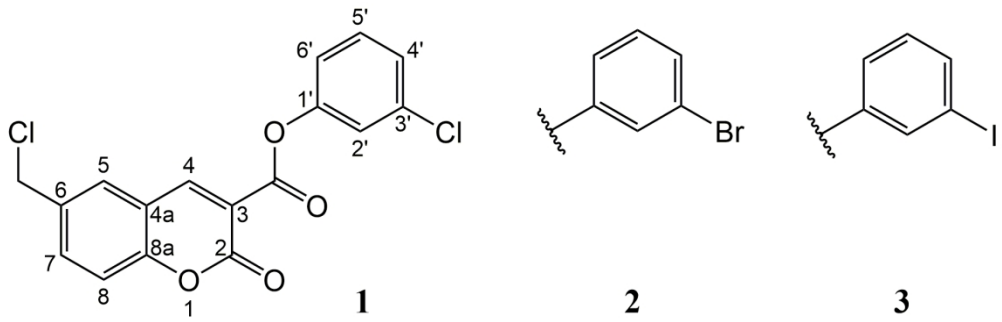

1 **2** **3**

IC_{50}* = 103 nM +/- 5 nM 65 nM +/- 3 nM 77 nM +/- 3 nM

Figure 1

167x62mm (300 x 300 DPI)

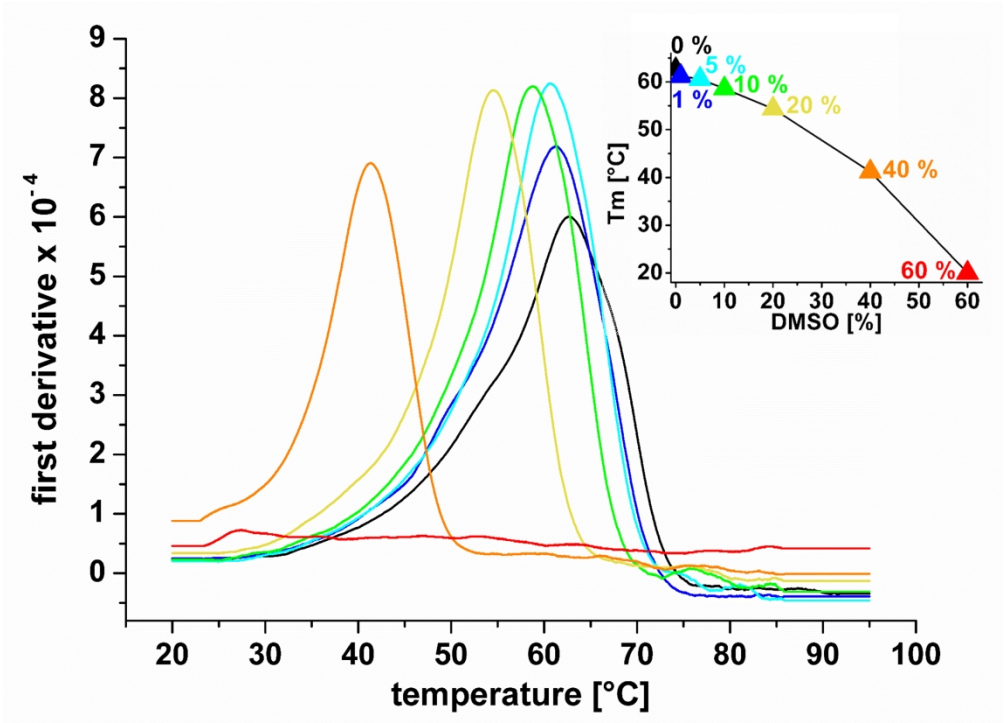

Figure 2

981x705mm (72 x 72 DPI)

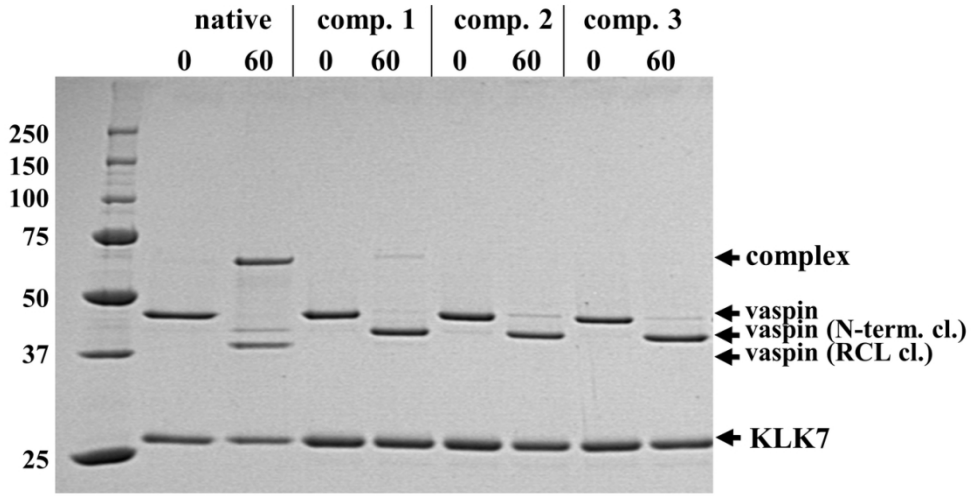

Figure 3

118x60mm (300 x 300 DPI)

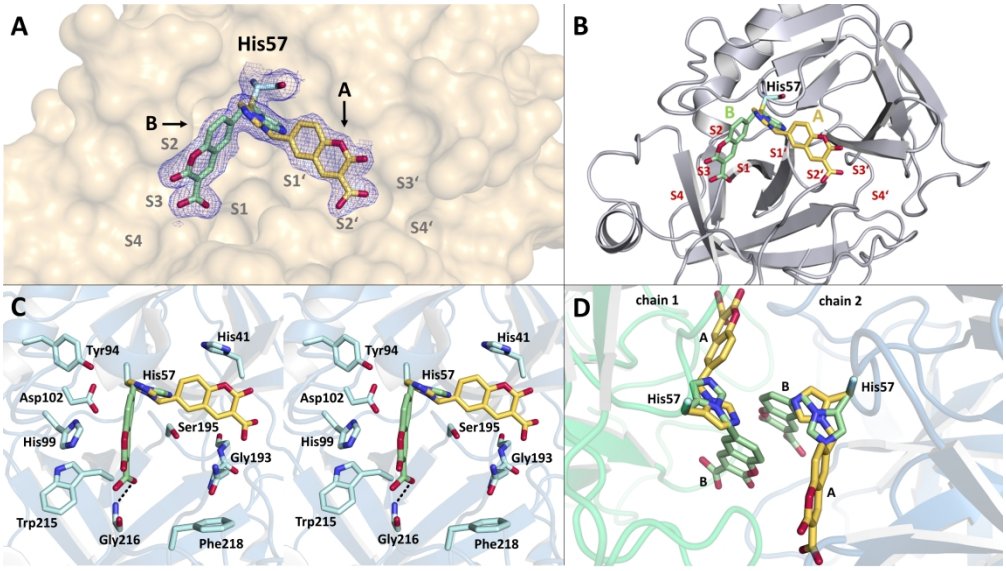

Figure 4

338x190mm (300 x 300 DPI)

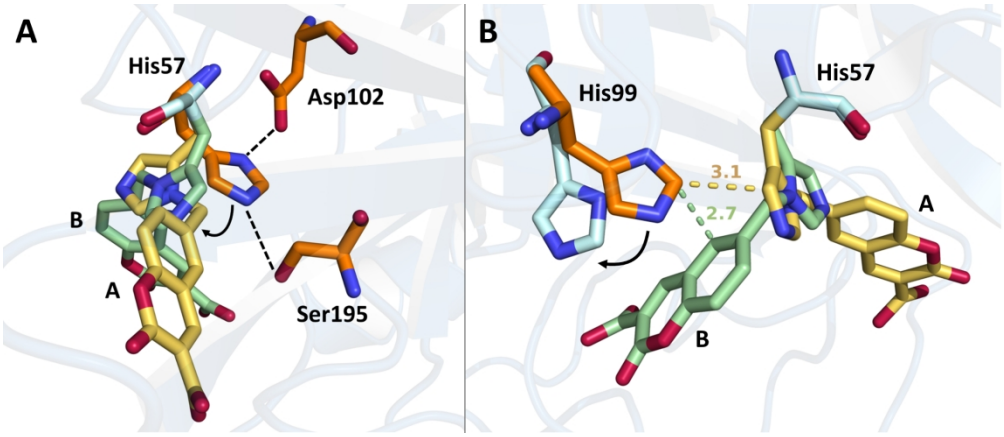

Figure 5

203x87mm (300 x 300 DPI)

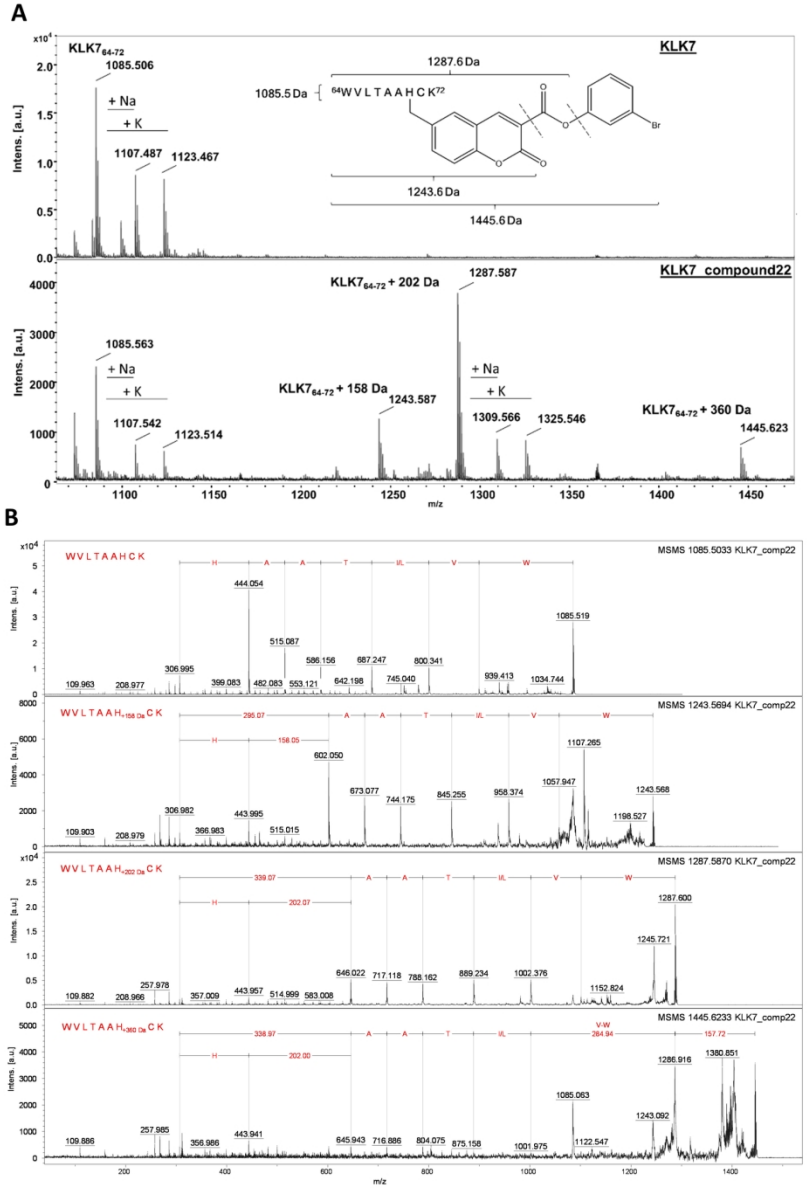

Figure 6

131x190mm (300 x 300 DPI)

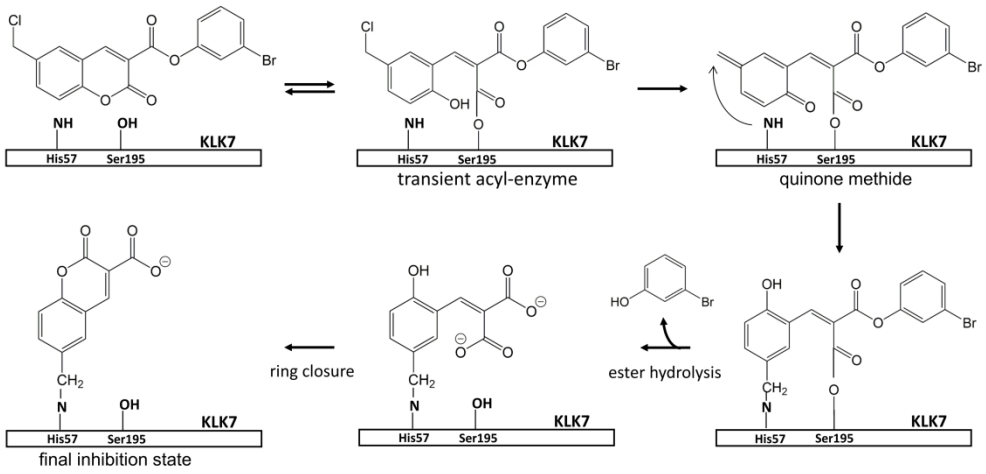

Figure 7

313x154mm (300 x 300 DPI)